B-7.4 Study on modeling temporal and spatial variation of partial pressure of CO_2 in the North Pacific utilizing data from ship-of-opportunity observation

Contact Person Yukihiro Nojiri
Head, Global Warming Mechanism Research Team,
Global Environment Research Group,
National Institute for Environmental Studies, Ministry of Environment
16-2, Onogawa, Tsukuba, Ibaraki 305-0053, Japan
Tel: +81-298-50-2499 Fax: +81-298-50-2569
E-mail nojiri@nies.go.jp

Budget for FY 1996-FY2000 65,415,000 Yen (FY2000; 14,461,000 Yen)

Abstract The ocean surface pCO_2 data set obtained by the ship-of-opportunity observation program by National Institute for Environmental Studies (NIES) utilizing cargo ships in the North Pacific was analyzed. The seasonal functions of ΔpCO_2 (pCO_2 difference of ocean and atmosphere) was obtained for each oceanic grid and monthly North Pacific ΔpCO_2 distribution maps were created. The seasonality of ΔpCO_2 showed significant difference for the region. March maximum and September minimum were observed in the subarctic Northern Western Pacific and Bering Sea. The summer decrease of pCO_2 is due to the biological production and increase in winter to the vertical mixing. Mid latitude North Pacific showed May maximum and November minimum, which has larger effect of seawater temperature change. Except for the north margin of the North Pacific is the net sink of atmospheric CO_2. The combination of the ocean surface wind data set by satellite observation and the maps obtained in this study gave an estimation of the CO_2 flux of 0.24GtC/y over the North Pacific, north of 34°N. The relationship between pCO_2 seasonality and nutrient concentration, which was also observed by the ship-of-opportunity program, were analyzed to characterize the biological productivity in the North Pacific.

Key Words CO_2, partial pressure in seawater, North Pacific, time series measurement

1. Introduction

Ocean pCO_2 observation is one of the ways to identify the partitioning of anthropogenically emitted CO_2 between the atmosphere and ocean. The difference of pCO_2 between ocean and atmosphere and wind velocity give the CO_2 flux into or out from ocean with appropriate exchange coefficient of CO_2. The accurate estimation of oceanic CO2 flux needs ΔpCO_2 data set having enough spatial and temporal coverage. However, there is no ocean basin having ΔpCO_2 data set with complete seasonal coverage. The ship-of-opportunity observation by NIES from 1995 is a unique ΔpCO_2 data set, which has

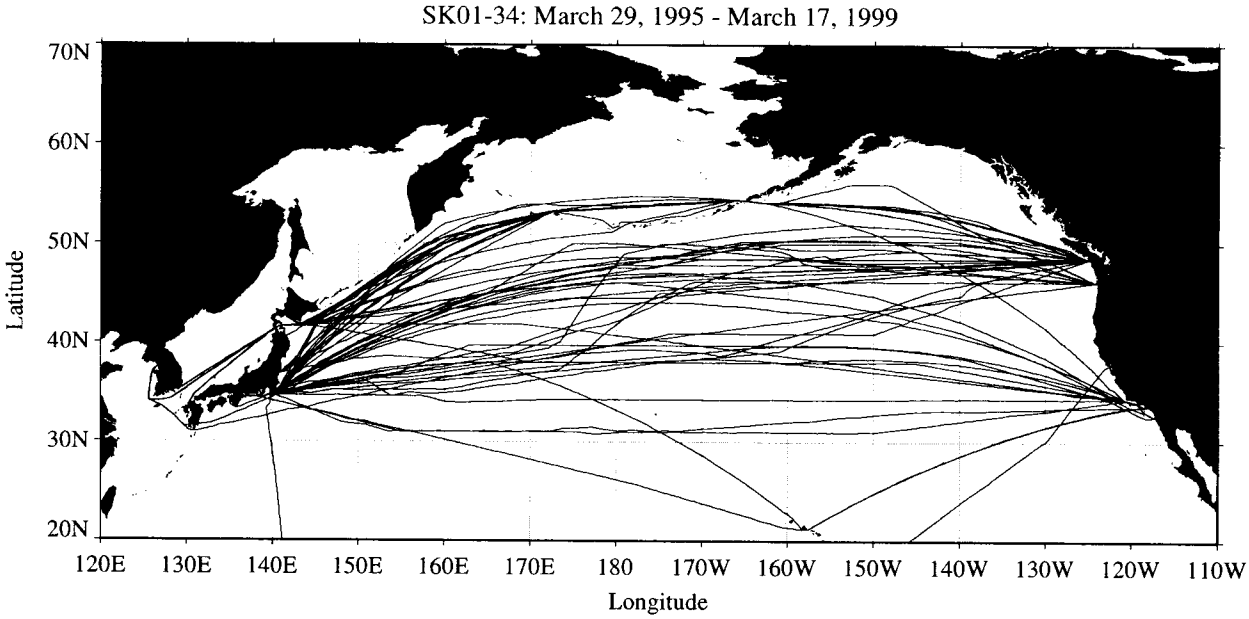

Fig. 1 M/S Skaugran cruise track form March 1995 to March 1999. The data north of 34°N were used for the mapping of ΔpCO_2 and flux estimation.

coverage for North Pacific with reasonable temporal resolution. In this study, the ΔpCO_2 data analysis provided the first detailed geographical view of monthly changes in ΔpCO_2 over a large region of the North Pacific. CO_2 net flux was estimated using the monthly maps.

2. ΔpCO_2 mapping

CO_2 measurements were made using continuous underway pCO_2 systems during 68 crossings aboard M/S Skaugran between March 1995 and March 1999. Most routes from North America to Japan were relatively constant, following a great circle path through the Gulf of Alaska, and Bering Sea, then southward along the Kuril Islands. Routes from Japan to North America ranged between 34°N and 50°N in the central North Pacific, except two passing though Hawaii and one going from the U.S. to Australia and then to Japan (Fig. 1). The mole fraction of CO_2 (xCO_2 in ppm) was measured every minute for seawater, and hourly for the air. The partial pressure of CO2 (pCO_2 in μatm) in seawater was calculated from measured xCO_2 with warming correction. The minute data were averaged for 5-degree longitude bins. The harmonic function was applied to the ΔpCO_2 data for each oceanic grid in the North Pacific, which has one and half year frequency.

$$\Delta pCO_2(t) = a + b\sin(2\pi t) + c\cos(2\pi t) + d\sin(4\pi t) + e\cos(4\pi t) \quad (1),$$

where t is time in year. In Fig. 2, the seasonal function for the 175°W meridian with observed data points were shown as an example. The monthly distribution maps of ΔpCO_2 were constructed by calculating monthly means for selected bands in a longitudinal section and interpolating those means to have the one-degree resolution of ΔpCO_2.

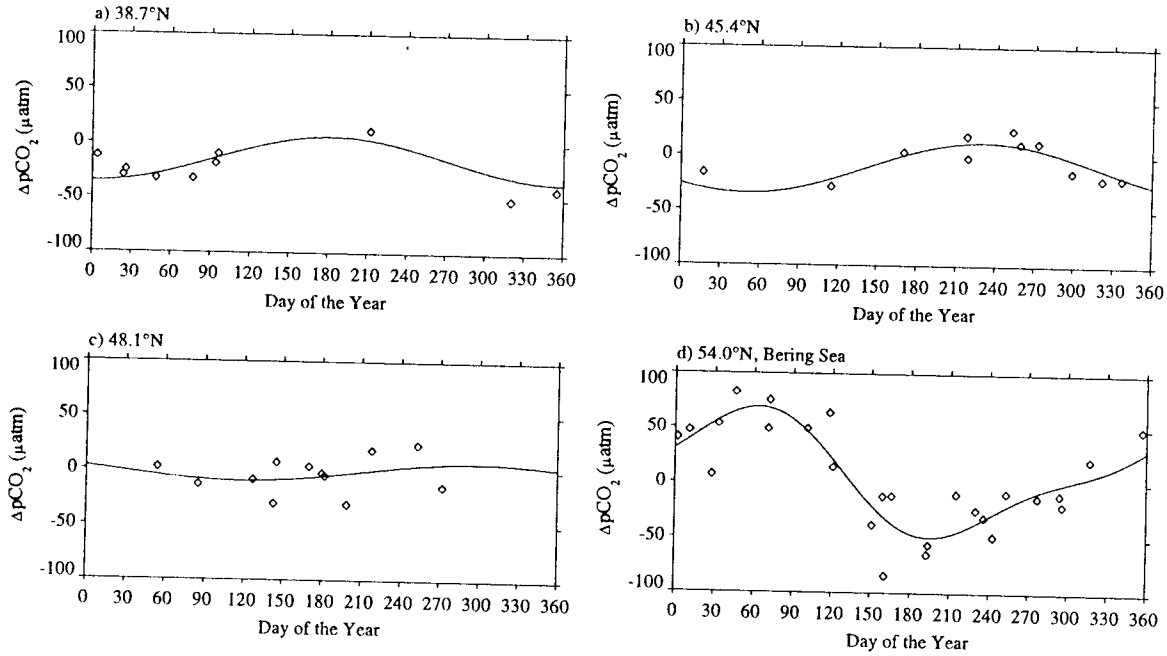

Fig. 2 Seasonal functions of ΔpCO_2 for four latitudinal bands in the 175°W longitudinal section: A. 38.7°N; B. 45.4°N; C. 48.1°N; and D. 54.0°N. The solid line shows the seasonal function fit by equation (1) and symbols the observed data.

The monthly distribution maps of ΔpCO_2 show clear unsynchronized patterns of ΔpCO_2 changes for different regions in the North Pacific. In winter (January to March), seawater pCO_2 in South Bering Sea, off Kamchatka island, and off Krill islands are higher than in the atmosphere (by up to 80 μatm) due to vertical mixing. In the rest of the North Pacific, ΔpCO_2 is negative (up to 60 μatm) as a result of cooling. Starting in April, the reduction of dissolved inorganic carbon in seawater from photosynthesis causes large decreases of pCO_2 in the marginal regions (off Kuril Islands, South Bering Sea, and North American coast), up to 90 μatm near Alaskan Peninsula. The pCO_2 in the central basin gradually increases during spring, becoming nearly zero by June. During summer (July-September) the marginal region and South Bering Sea remain undersaturated. Undersaturation in the marginal regions decreases as warming continues. The central basin remains near equilibrium, although a region of significant oversaturation (up to 50 μatm) develops off the coast of North American and extending to approximately 155°W to the west. In autumn, seawater pCO_2 decreases due to the cooling of sea surface waters, except for Bering Sea where vertical mixing starts as early as late October. The remainder of the basin is undersaturated.

3. Air-sea CO_2 flux

The air-sea flux of CO_2 was calculated based on the equation of Wanninkhof, and wind data by SSMI satellite for the observed period of M/S Skaugran. Both oceanic efflux and influx are strongest in winter. This is partly due to ΔpCO_2 distributions and partly to high monthly

wind velocities (up to 11 m s^{-1}) in this season. In contrast to large spatial variations of CO_2 flux in winter, fluxes in spring and summer are much uniform in most regions. Even though low ΔpCO_2 up to -100μatm occurs in June to July near the Alaska Peninsula and area off Kril Islands and high ΔpCO_2 up to 60 μatm occurs in August to September off California coast, fluxes in these regions are only slightly different from other regions, because the monthly wind is weakest in summer (as low as 6 m s^{-1}). Results of annual CO_2 fluxes are shown in Table 1. On the annual base, South Bering Sea and off Kamchatka island are significant CO_2 sources because both the CO_2 oversaturation and wind speed are high in winter. The remainder of the NNP is a sink for CO_2. The north-south difference in the net annual sink is much smaller in the eastern Pacific of observation area than that in the west. The integrated fluxes for North Pacific north of 34°N are 0.24GtC y^{-1}, which is about twice as high as the average ocean. Integrated fluxes clearly show that the CO_2 exchanges in winter and autumn play the main role in the net annual CO_2 flux. In winter and autumn, CO_2 intake by the mid latitude zone (35°N-45°N) is much higher than that by the high latitude zone (45°N-55°N). The sum of autumn and winter uptake by the mid latitude zone is 0.198GtC, which is close to the annual intake of the whole area. The mid latitude zone is a much stronger CO_2 sink than the high latitude zone.

Table 1 Integrated annual CO_2 fluxes (MtC y^{-1}) in the North Pacific obtained from the analysis of M/S Skaugran observation of pCO_2. Negative value is the net oceanic sink of CO_2. The first sum in the right column is total flux between 45°N and 55°N, the second the total flux between 35°N and 45°N, and third the total flux of the whole monitoring area. The first sum in the last row is the total flux between 145°E and 175°E, the second the total flux between 175°E and 205°E, and the third the total flux between 205°E and 235°E.

	145-160°E	160-170°E	170°E-170°W	170-150°W	155-140°W	140-120°W	sum
50-55°N	0.0	6.8	9.1	-6.6	-3.3	-3.0	
45-50°N	-1.5	0.9	-6.5	-13.0	-11.4	-11.4	-39.9
40-45°N	-13.6	-15.0	-15.7	-18.1	-14.3	-9.1	
35-40°N	-30.3	-27.1	-19.4	-21.2	-14.9	-5.0	-203.7
Sum		-79.8		-91.4		-72.4	-243.6